Autonomous Ultrasonic Thickness Measurement of Steel Bridge Members using a Climbing Bicycle Robot

Yu Otsuki[1], Son Thanh Nguyen[2], Hung Manh La[3], and Yang Wang[4, *]

[1]School of Civil and Environmental Engineering, Georgia Institute of Technology,
790 Atlantic Drive NW, Atlanta, GA, USA, *yu.otsuki@gatech.edu*

[2] Department of Computer Science and Engineering, University of Nevada, Reno,
1664 N Virginia St, Reno, NV, USA, *thanhson@nevada.unr.edu*

[3] Department of Computer Science and Engineering, University of Nevada, Reno,
1664 N Virginia St, Reno, NV, USA, *hla@unr.edu*

[4] School of Civil and Environmental Engineering & School of Electrical and Computer Engineering, Georgia Institute of Technology,
790 Atlantic Drive NW, Atlanta, GA, USA, *yang.wang@ce.gatech.edu*

Abstract: This paper presents the development of a steel-climbing bicycle robot integrated with an ultrasonic sensing device towards autonomous thickness measurement of steel bridge members. The bicycle-like robot has two magnetic wheels controlled by two independent steering actuators, which navigates on various steel surfaces (flat, curved, rough, concave, and convex). The compact ultrasonic sensing device is capable of high-voltage pulse excitation, filtering/amplification of the received ultrasonic signal, and high-speed analog-to-digital conversions (up to 80 MHz). Along with the ultrasonic sensing device, the robot carries a dual element transducer, an automatic gel couplant dispenser, a position tracking sensor, and a camera. A mounting/retrieving mechanism of the transducer is designed to ensure the reliable contact of the transducer on steel surfaces. The camera view assists an operator to safely navigate the robot to measurement locations, properly dispense gel couplant, and firmly press the transducer on a measurement surface. The automated robot localization provides accurate thickness measurement locations, which are mapped real-time in 3D space together with the robot's travel path. We validate the performance of the developed system in several indoor and outdoor tests. A supplementary video demonstrating the robot's maneuverability and ultrasonic thickness measurements is available on YouTube: https://youtu.be/aCt0BZnxKVc.

Keywords: autonomous inspection, ultrasonic thickness measurement, steel climbing robot, wireless sensing, non-destructive testing

Introduction

According to the National Bridge Inventory (FHWA 2016), about 30% of the nation's bridges are steel or steel-continuous bridges. As mandated by the Federal Highway Administration, biennial bridge inspections are performed. Current inspections are primarily a visual activity, requiring an inspector to reach within arm's length to a structural member surface for a thorough examination. The inspection process can be labor-intensive and often entails expensive snooper trucks or lane closures. While human inspection is necessary, the latest robotics and information technologies can be adopted to ease inspection efforts and provide additional data for bridge condition assessment (Wang *et al.* 2022). Robotic structural inspection can be achieved by integrating a mobile robot with sensing tools (Ahmed *et al.* 2020). Acceleration measurements have been successfully obtained by a mobile robot for system identification (Matarazzo and Pakzad 2016; Zhu *et al.* 2012). Surface crack detections on bridges can be automated by a mobile robot equipped with vision sensors (Oh *et al.* 2009; Sutter *et al.* 2018). A comprehensive mobile robot with a laser scanner, cameras, sensors for non-destructive testing has been developed for autonomous bridge deck inspection (La *et al.* 2013). Furthermore, attempts have been made recently to utilize moving vehicles for bridge health monitoring (Malekjafarian *et al.* 2022; Matarazzo *et al.* 2022).

A steel bridge can be a complex engineering structure made up of various members such as I-beams, hollow tubes, round tubes, diaphragms, joints, and bolts, among others. Therefore, developing a climbing robot that can work on any surface is a challenging task. A conventional design for a steel climbing robot includes wheeled robots (Pham and La 2016; Sirken *et al.* 2017; Zhu *et al.* 2012) and tank-like tracks (Nguyen and La 2019a), but such designs may face difficulties on complex surfaces and tight spaces on steel bridges. Some other notable locomotion mechanisms inspired by animal motions have been developed, such as a roller-chain robot (Nguyen and La 2019b), a spider-like robot (Bandyopadhyay *et al.* 2018), an inchworm-like robot (Ward *et al.* 2014), a legged robot (Mazumdar and Asada 2009), and a hybrid robot (Nguyen *et al.* 2020). However, such intricate mechanisms require complicated control with multiple joints and motors, and thus may not be suitable on bridge members with complex geometries and oftentimes narrow space between members to navigate through. One novel approach recently developed by the authors (Nguyen *et al.* 2022) is a multi-directional bicycle robot that is mechanically simple, but able to navigate on various steel surfaces (flat, curved, rough, concave, and convex) as often seen in steel bridges.

Aside from robotics, non-destructive testing is one of the well-established methods for the detection of structural damage and deterioration. One major technique in non-destructive testing is the use of ultrasonic signals, which employs a transducer to generate excitation and measure response as shown in Fig. 1.When no internal defect exists, an ultrasonic wave launched on one surface of a metal plate is reflected by the other surface (back wall). According to the timing of the received signal, referred to as Time of Flight (ToF), the thickness of the plate can be estimated. The measured thickness value is primarily intended for measuring corrosion-induced thickness loss of steel members. By comparing the measured thickness with the nominal thickness, or with a previous measurement if it were performed, it is possible to detect and quantify thickness change due to corrosion. Note that between the transducer and the specimen, some couplant such as gel is placed to facilitate the propagation of solid waves. Unlike climbing robots, there have been some notable developments on unmanned aerial vehicles equipped with a transducer for ultrasonic thickness measurements (González-deSantos *et al.* 2019; Mattar and Kalai 2018; Zhang *et al.* 2018; Zhang *et al.* 2022). Such developments, however, are intended for wall-thickness measurements on large oil storage tanks or vessels with easy flight access.

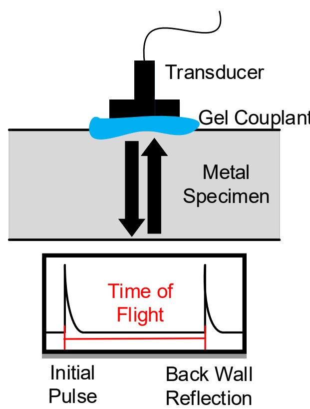

Fig. 1. Ultrasonic thickness measurement

Over the past few decades, the development of sensing technologies by the structural health monitoring community has enabled continuous and reliable monitoring of the condition of civil engineering structures. As the latest generation of low-cost compact wireless sensing devices, the *Martlet* (Kane *et al.* 2014) platform provides a novel sensing solution for various kinds of structural health monitoring applications, including strain, acceleration, and displacement measurements (Liu *et al.* 2016), ultrasonic surface crack detection (Chen *et al.* 2016), bridge weigh-in-motion at an in-service highway bridge (Lander *et al.* 2022), and integration with unmanned aerial vehicles (Zhou *et al.* 2022). For ultrasonic thickness measurement, the authors (Otsuki *et al.* 2021) recently developed a compact *Martlet* ultrasonic device that consists of two daughter boards: a high-rate ultrasonic board and a pulser board. This compact ultrasonic device has been designed to be readily integrated with a mobile robot for autonomous structural inspections.

Marrying the two state-of-the-art developments (Nguyen *et al.* 2022; Otsuki *et al.* 2021), this paper presents the novel design of a steel-climbing bicycle robot for the autonomous inspection of steel bridges. A detailed literature search has not identified similar work that mounts an ultrasonic thickness measurement device on a small tetherless climbing robot for steel bridge inspection, letting alone validating the system in the field. In comparison, this work generated the first-of-its-kind small-footprint robot with not only the ability to navigate on various steel surfaces, but also the capability of ultrasonic transducer deployment/retrieval, gel dispensing, and high-rate ultrasonic data collection that enables accurate steel thickness measurement. Field validations are performed on different structures including a steel-girder bridge, a square tube structure, and rough/rusted surface measurements.

The remainder of this paper is organized as follows. The design and development of the *Martlet* ultrasonic device and the bicycle mobile robot are first presented, along with the hardware and software integration scheme of the two devices. Several indoor and outdoor tests next validate the successful operation and accuracy of the ultrasonic thickness measurement by the developed mobile robot.

Martlet ultrasonic sensing device

Design and development

This section provides a brief overview of the *Martlet* ultrasonic thickness measurement device that consists of the two daughter boards: the high-rate ultrasonic board (Otsuki *et al.* 2021) and the pulser board (Otsuki *et al.* 2022a). Fig. 2 shows the functional diagram.

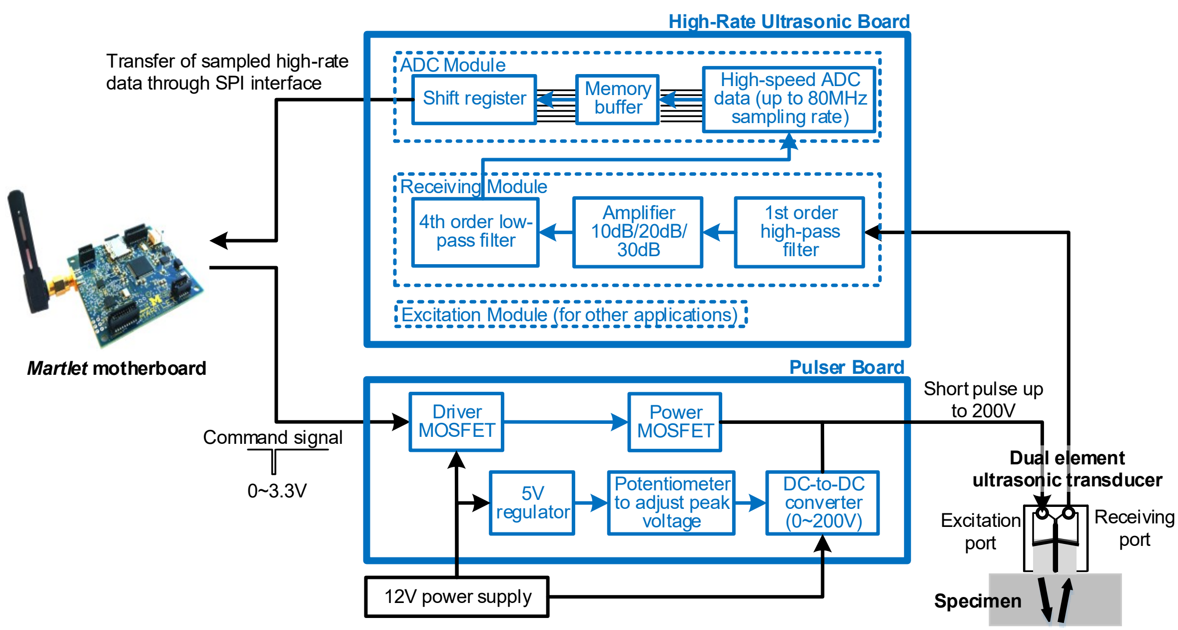

Fig. 2. Functional diagram of the *Martlet* ultrasonic thickness measurement device

The high-rate ultrasonic board consists of three modules: the excitation module, the receiving module, and the analog-to-digital converter (ADC) module. The excitation module was designed for launching surface waves and is not utilized in this study for thickness measurement. Instead, the pulser board serves as the transducer excitation source for measuring specimen thickness. The receiving module conditions the signal received from a transducer through a 1st-order high-pass filter, amplitude amplification (10dB/20dB/30dB), and a 4th-order low-pass filter. Among the commonly used standard filter types, Bessel type is selected for the 4th-order low-pass filter that is critical for the signal conditioning performance. Bessel filters offer a linear phase performance and help maintain the signal waveform in the time domain (Horowitz and Hill 1989), which assists in accurately identifying the ToF of the received signal. The filtered and amplified signal is then sampled by the high-speed ADC module with a sampling frequency up to 80 MHz. The sampled data is transferred to the *Martlet* motherboard through a serial-peripheral-interface (SPI) connection. In the end, the *Martlet* motherboard wirelessly sends the data to a base station connected to a PC.

When the ultrasonic solid wave propagates into the specimen, the amplitude of the ultrasonic signal decreases as the wave reflects multiple times between the two surfaces of the specimen. A larger amplitude of the signal is preferred to ensure a good signal-to-noise ratio that results in more accurate thickness measurement. For this purpose, a compact pulser board has been developed to generate a short-pulse excitation at high voltage. The high voltage DC-to-DC converter enables the excitation voltage to be increased up to 200V. The voltage can be easily adjusted by an onboard potentiometer. The driver MOSFET is a type of power amplifier that accepts a low-power command signal from a microcontroller on the *Martlet* and produces a high-current drive input for the gate of the power MOSFET. The power MOSFET initiated by the high-current drive input achieves the fast-switching time required by the pulse excitation. Note that the pulser board requires a 12V power supply that is common in robotics and can be readily integrated with a mobile robot for autonomous inspection. An example pulse excitation signal generated by the developed pulser board can provide a 200 V pulse with about 1 μs duration. With this high excitation voltage, the ultrasonic signal can achieve a better signal-to-noise ratio, which helps improve the accuracy of the ultrasonic thickness measurement.

Fig. 3 shows the printed-circuit-board (PCB) design of the *Martlet* ultrasonic thickness measurement device that consists of the *Martlet* motherboard, the high-rate ultrasonic board, and the pulser board. The planar dimension of the motherboard is 63.5 mm × 59.7 mm. The pulser and high-rate ultrasonic boards can stack on top of the *Martlet* motherboard through the four corner connectors. The device connects with a dual element transducer that has both excitation and receiving ports (Fig. 2).

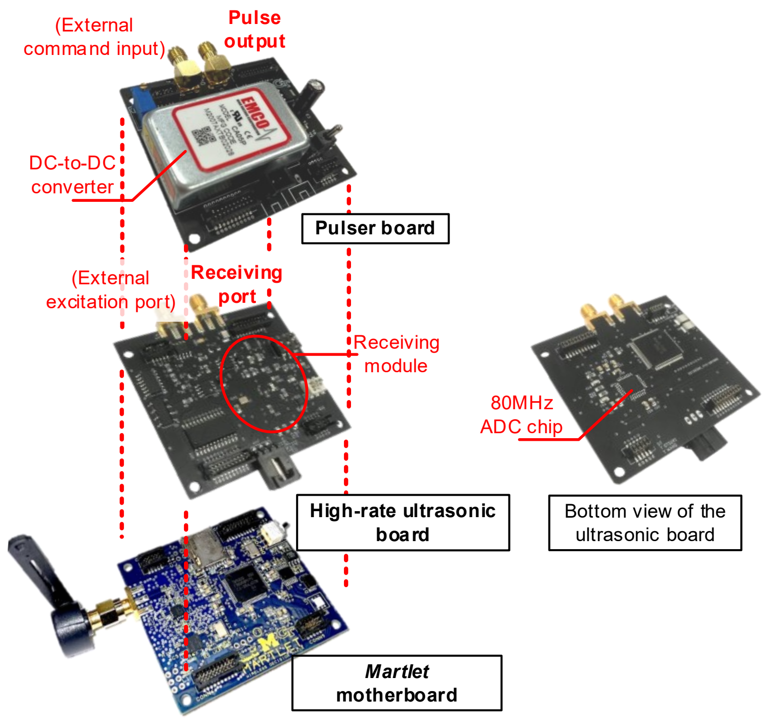

Fig. 3. PCB design of the *Martlet* ultrasonic thickness measurement device

Thickness measurement validations

Before integrating the developed *Martlet* ultrasonic device with a mobile robot, we validate its measurement accuracy through a field test on a steel girder bridge near LaGrange, GA, USA (Fig. 4). A 2.25 MHz dual element transducer is used for this test and connected with the *Martlet* ultrasonic device. An oil couplant is applied between the transducer and the specimen to achieve better transmissibility of the ultrasonic signal. According to the structural design documents, the steel girder utilizes ASTM A36 carbon steel with a W36×135 section. The nominal thickness of the W36×135 section is 20.32 mm (0.80 inch) for the bottom flange and 15.24 mm (0.60 inch) for the web. Sand and dust have accumulated on the surface of the bottom flange, as is often the case in practice (Kulicki *et al.* 1990) and make the thickness measurement more challenging compared to the clean surface of the web. The entire girder has paint coatings. Due to the presence of coatings, the apparent thickness is larger than the nominal thickness of the steel itself. Therefore, instead of conducting velocity calibration by caliper measurements, this study uses the nominal velocity of ultrasonic signals. Note that the nominal velocity depends on the material property and is 5.94 mm/μs for carbon steel

(Aquil and Leonard 2018). One of the advantages of ultrasonic thickness measurement is that it does not require the removal of coatings to estimate the metal thickness, because the ultrasonic signal reflects on the interfaces between the metal and coating.

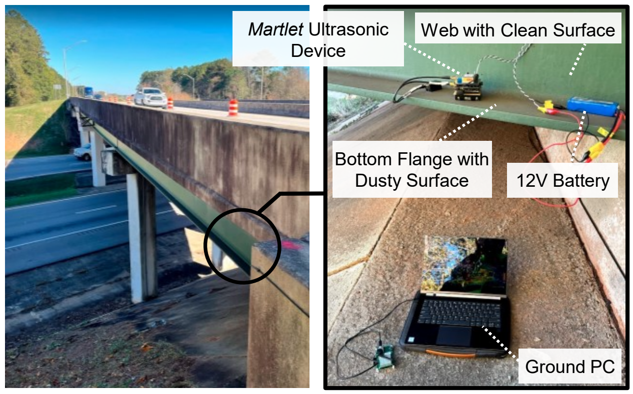

Fig. 4. Thickness measurement on a steel bridge girder near LaGrange, GA, USA

Fig. 5(a) shows the received signals of the 2.25 MHz dual element transducer sampled by the high-rate ultrasonic board for the 15.24-mm-thick web with clean surface. The received signal includes a sequence of echoes, which are the reflections of the ultrasonic waves created by the transducer. The time interval between the neighboring echoes is the ToF. To accurately obtain the ToF, we calculate the autocorrelation function of the received signal using the following equation:

$$a[k] = \sum_{l=0}^{N-k} v[k+l]v[l], \quad k = 0, \dots, N \tag{1}$$

where $a[k]$ is the autocorrelation function at discrete-time lag k; $v[l]$ is the received voltage signal at the time step l; N is the total number of data points. Based on the peak value of the autocorrelation function, the ToF is identified as 5.08 μs for the web. Although alternatively, one could estimate the ToF using the time difference between the first and second peaks in the received ultrasonic signal, the use of the autocorrelation function is in general more robust against noise and with rough surface conditions.

Similarly, Fig. 5(b) shows the received signals and autocorrelation function for the 20.32-mm-thick bottom flange with dusty surface. Note that we did not clean dust on the bottom flange. Therefore, autocorrelation waveforms are slightly distorted compared to the web due to the layer of dust. However, the peak is clearly identified at 6.82 μs.

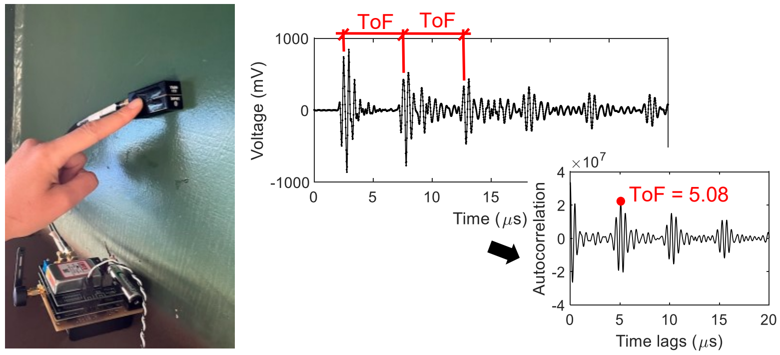

(a)

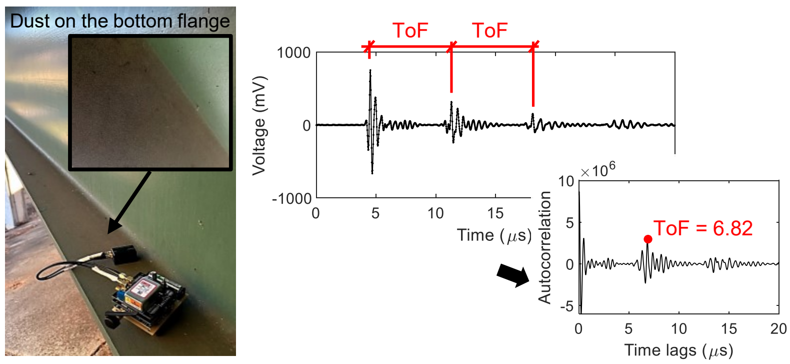

(b)

Fig. 5. Received signals and autocorrelation function: (a) 15.24-mm-thick web with clean surface; and (b) 20.32-mm-thick bottom flange with dusty surface

The thickness of each specimen is calculated by Eq. (2) and summarized in Table 1.

$$\text{Thickness} = \frac{\text{ToF} \times \text{Nominal Velocity}}{2} \tag{2}$$

For the 15.24-mm-thick web, the estimated thickness is 15.09 mm. The difference from the nominal thickness of 15.24-mm is only -0.15 mm (-0.99%). For the 20.32-mm-thick bottom flange, the estimated thickness is 20.26 mm, only -0.06 mm (-0.30%) different from the nominal thickness of 20.32 mm. In general, actual thickness values may vary from the nominal value within an allowable tolerance, as specified by (ASTM-A6/A6M-14 2014). The measurements obtained both on the dusty web and the clean flange are well within their allowable tolerance of 0.76 mm from the corresponding nominal thickness. Therefore, this field test validates the performance of the developed *Martlet* ultrasonic device in the presence of coatings and accumulated dust on the steel surface. The *Martlet* ultrasonic device is ready for integration with a mobile robot for steel bridge inspection.

Table 1. Thickness measurement results on a steel girder bridge

Specimen	15.24-mm-thick web (clean)	20.32-mm-thick bottom flange (dusty)
ToF	5.08 µs	6.82 µs
Nominal velocity	5.94 mm/µs	5.94 mm/µs
Estimated thickness	15.09 mm	20.26 mm
Difference from nominal thickness	-0.99%	-0.30%

Steel climbing bicycle robot integrated with *Martlet* wireless ultrasonic device

Robot design

This section presents the compact design of a multi-directional bicycle robot for maneuvering on complex-shaped ferromagnetic structures. Fig. 6 illustrates the design concept. Inspired by a bicycle, two revolute joints equip the robot with two independent steering actuators, which greatly increase the multi-directional maneuverability. The wheels are embedded with permanent ring-shaped magnets to generate large adhesive forces on steel structural members. The high maneuverability of the two steering actuators allows the robot to operate with two different modes: a bicycle-like mode and a multi-directional mode. In the bicycle-like mode, either only the front steering unit is activated (Fig. 6(a)), or only the rear steering unit is activated (Fig. 6(b)). With this mode, the robot can easily change the traveling direction when moving on narrow surfaces of a steel member. In scenarios that require sideway movements, the multi-directional mode is enabled, which activates both steering units simultaneously as shown in Fig. 6(c).

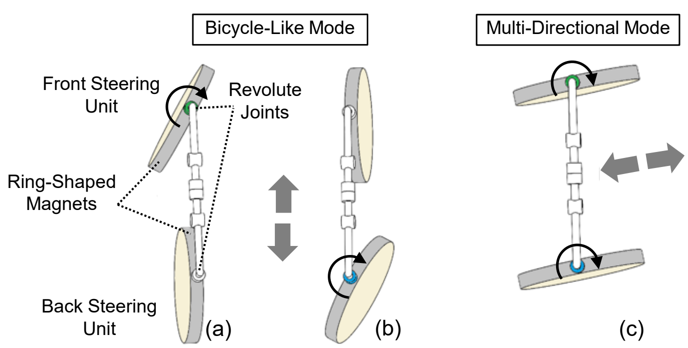

Fig. 6. The design concept demonstrating the maneuverability of our robot; (a) bicycle-like mode: only the front steering unit (green) is active; (b) bicycle-like mode: only the rear steering unit (blue) is active; and (c) multi-directional mode: both front (green) and rear (blue) steering units are active

In addition to the steering revolute joints, a passive rotary joint is installed as a dynamic connection between two halves of the robot's body as shown in Fig. 7. This rotary joint provides one more degree of freedom (DOF) so that the two halves of the body can rotate relative to each other along the axial direction. To offer the two half bodies with necessary postures for navigating on certain terrains, the joint is designed to be passive and has no actuation (unlike the steering revolute joints). When needed by the postures of the two half bodies to accomplish steering and driving motions on these terrains, the rotation happens naturally. For example, this additional DOF allows both wheels to adhere well on unusual surfaces, such a convex corner transition in Fig. 7(a), a convex cylindrical surface in Fig. 7(b), and a concave cylindrical surface in Fig. 7(c).

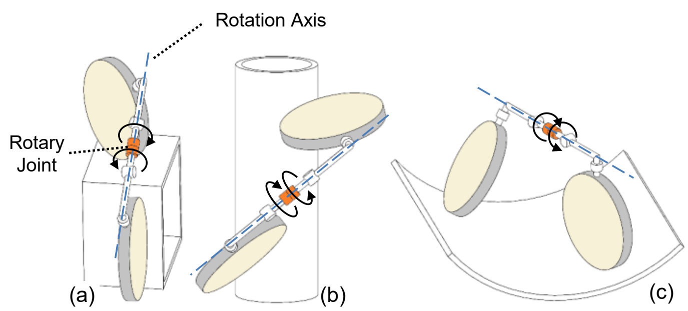

Fig. 7. The demonstration of a rotary joint (orange) providing effective adherence to uneven surfaces: (a) a convex corner transition; (b) a convex cylindrical surface; and (c) a concave cylindrical surface

Fig. 8 demonstrates the locomotion mechanism on more terrains. In the bicycle-like mode shown in Fig. 8(a)-(d), only one steering unit is active. This mode allows the robot to travel on structures with limited and narrow contacting areas or reverse the direction immediately without turning (Fig. 8(a)). In addition, the robot can turn on the spot by stopping the rear wheel and driving the front wheel (Fig. 8(b)). Furthermore, the robot can comfortably climb two intersecting surfaces by virtue of its rotary joint and two independent steering units (Fig. 8(c). Fig. 8(d) shows that the robot can stride and pass over a narrow edge, as long as the edge is thicker than the nearest space between its two wheels.

In the multi-directional mode as demonstrated in Fig. 8(e)-(f), both two steering units are active. With both wheels in parallel and driving in the same direction, the robot can move spirally around a cylinder or move sideways. When two wheels drive in opposite directions, the robot can rotate around its body center. Weblink to a video illustration of the robot's sophisticated maneuverability can be found in the Data Availability Statement.

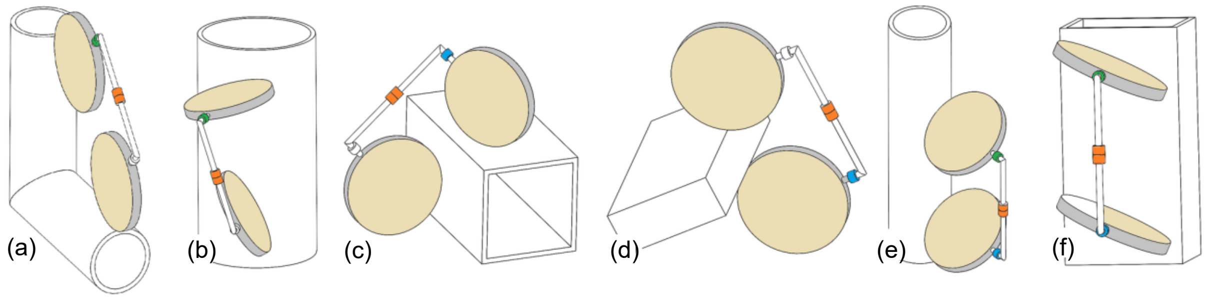

Fig. 8. Two modes of the bicycle mechanism: (a)-(d) only one steering unit is active (bicycle-like mode); and (e)-(f) two steering units are active (multi-directional mode)

Fig. 9 shows the 3D design of the bicycle robot. Fig. 9(a) describes each component. The robot's dimension is 150 mm × 80 mm × 90 mm. The frame is 3D-printed using ABS (acrylonitrile butadiene styrene) plastic. The ABS plastic is lightweight and strong enough to provide the weight/adhesive forces needed in the validation tests. The ring magnets each produce 250 N of adhesive force and are placed at the cores of the two wheels. Each magnetic wheel is driven by a high-torque gear DC driving motor (100kg·cm torque each) attached on the wheel side. On top of the fixture for each magnetic wheel, a revolute joint is installed and controlled by a steering servo (32kg·cm torque). The front and rear frames are linked by a bearing acting as the rotary joint. Fig. 9(b) shows the robot's pose when the rotary joint is in effective. Two halves of the robot body rotate against each other about the axis line. Note that with the wheel size employed in this study, the minimum member size that can be navigated upon is 100 mm in diameter for cylindrical types, and 50 mm wide for flat surfaces.

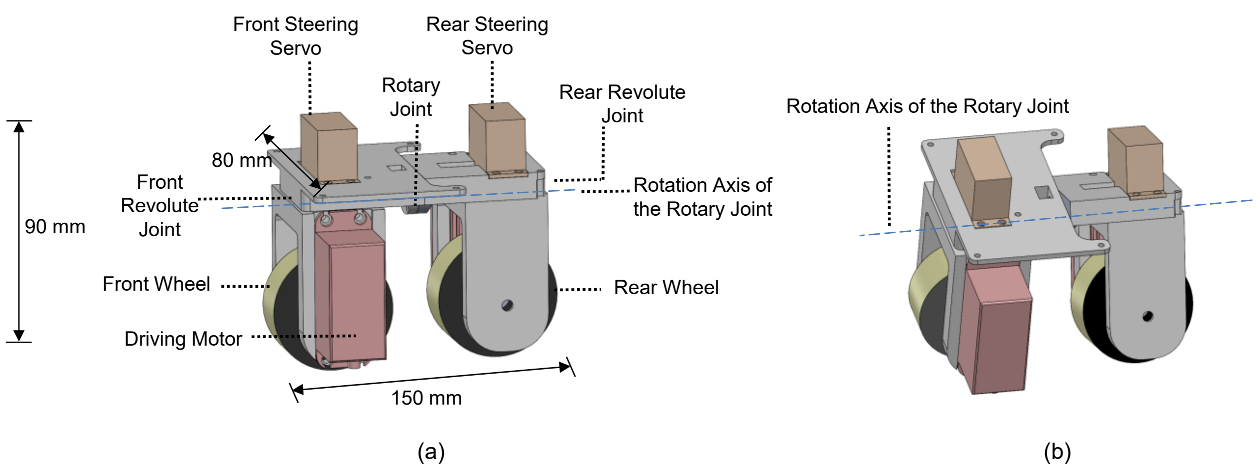

Fig. 9. 3D design model of the robot: (a) components and dimensions; and (b): the passive rotary joint allows two halves of the robot body rotation against each other

Transducer deployment and couplant pumping mechanisms

To integrate the functionality of ultrasonic thickness measurement on the robot, the mechanisms of transducer deployment and couplant pumping are developed. Fig. 10 shows the transducer deployment mechanism. A four-bar mechanism is designed for generating vertical movements of the ultrasonic transducer, in order to place the transducer on a measurement surface and retrieve afterwards. A flexible layer of TPU (thermoplastic polyurethane) plastic is used together with an angle lock to avoid the overload of servo motors while providing a firm contact between the transducer and a steel measurement surface.

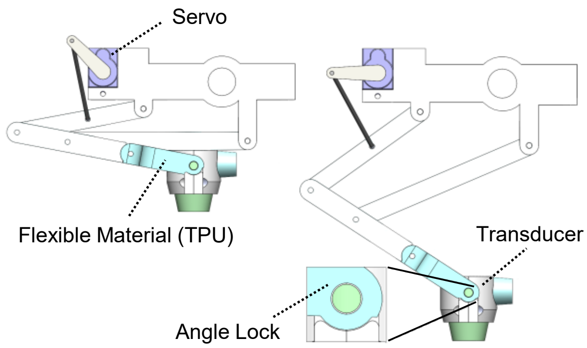

Fig. 10. Transducer deployment mechanism

A pumping mechanism of the gel couplant is illustrated in Fig. 11. Since a direct-contact transducer is used for thickness measurement, couplant is necessary to fill the air gap between the transducer and surfaces. A gel couplant with high viscosity (UltraSoniX from Echo Ultrasonics LCC) is selected. The gel couplant adheres well on surfaces of different orientations, including vertical walls and ceilings. The selected gel couplant is also water-soluble and environmentally friendly. Therefore, the gel can be easily washed off by rain and does not cause corrosion even when left on steel bridge surfaces. For mount on the robot, the gel couplant is stored in a syringe tank. A mini peristaltic pump with a silicone tube is utilized to release the high viscosity gel in a controlled manner.

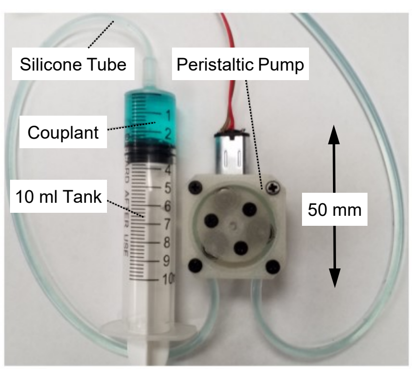

Fig. 11. Gel couplant pumping mechanism

Overall robotic inspection system

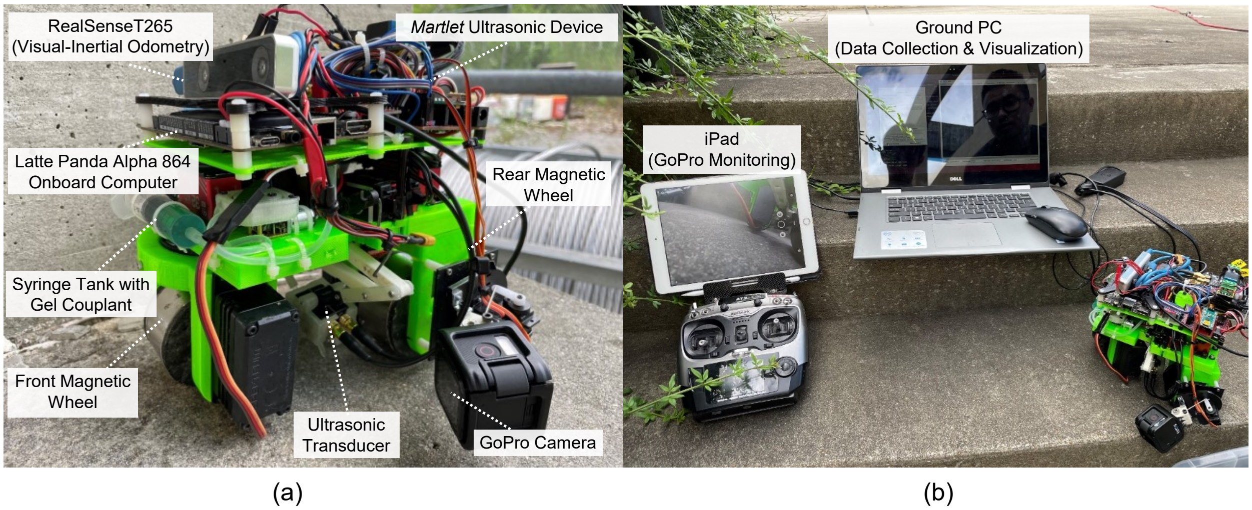

Fig. 12. Bicycle robot and ground control station: (a) bicycle robot integrated with sensors; and (b) ground control station consisting of two independent channels, i.e., 1) ground PC and 2) remote controller and monitor

Fig. 12 shows the robotic inspection system, including the bicycle robot integrated with the *Martlet* ultrasonic device and other devices (Fig. 12(a)), and the ground control station in Fig. 12(b). As shown in Fig. 12(a), the *Martlet* ultrasonic device is mounted on top of the robot. With the transducer deployment mechanism in Fig. 10, a 2.25MHz dual-element transducer is installed in the space between the two wheels. This location is ideal for protecting the transducer while traveling, and allows measurement that can take place on both flat and curved surfaces. In addition, robot localization is achieved using an Intel RealSense T265 tracking camera (Fig. 12(a)), which can provide real-time positions using visual-inertial odometry. The GoPro camera is installed next to the rear wheel. Depending on whether the robot is traveling or stopping for a thickness measurement, an operator can remotely control the rotational hinge on the GoPro support to change the camera orientation. This makes it possible to switch the GoPro view between the robot's front path and the transducer mounting/measurement position. An onboard computer, Latte Panda Alpha 864, is installed on the robot. The robot's weight is 1.2 kg. When powered by a 700mAh LiPo battery, a human operator can remotely control the robot to work for about 30 minutes.

As shown in Fig. 12(b), the ground control station consists of two independent channels, i.e., 1) ground PC and 2) remote controller and monitor. The robot's onboard computer is connected with the ground PC through a local WiFi network. The onboard computer and the ground PC form a Robot Operating System (ROS) network (Quigley *et al.* 2009). In our implementation, the ground PC acts as the master for data collection (from the robot's onboard PC) and visualization. The ultrasonic data received by the *Martlet* device is transferred to the onboard computer through a Universal Asynchronous Receiver/Transmitter (UART) interface. The robot position obtained by the RealSense T265 tracking camera is first stored in the onboard computer. The ultrasonic data and robot position are sent from the onboard computer to the ground PC. The ground PC matches and visualizes the thickness location and the robot position in 3D space in real-time. The robot locomotion is maneuvered remotely by a joystick via a radio connection. The iPad streams the GoPro video through a Bluetooth connection.

Thickness measurement validations by the mobile robot

Indoor thickness measurements

To validate the performance of the bicycle robot for thickness measurement, a laboratory test is first conducted at the Earthquake Engineering Laboratory, University of Nevada, Reno. We first verify the climbing capability of the mobile robot as shown in Fig. 13. The robot can smoothly navigate on different types of steel surfaces such as a square tube, a round tube, a concave transition, and a vertical surface (Otsuki *et al.* 2022b).

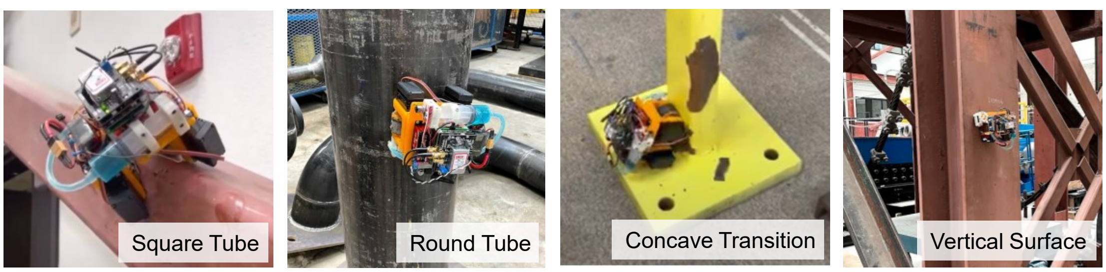

Fig. 13 Climbing on various steel structures

The ultrasonic thickness measurement is then conducted on a square steel tube with the nominal thickness of 11.81 mm (Fig. 14(a)). The steel member is made of ASTM A36 carbon steel, for which the nominal wave velocity of 5.94 mm/μs is used (Aquil and Leonard 2018). The robot is remotely operated to move to desired measurement locations, where the robot stops to apply gel couplant on the steel surface (Fig. 11), followed by transducer mounting (Fig. 10) and thickness measurement. Fig. 14(b) shows ultrasonic waveforms obtained by the robot. The autocorrelation function of the ultrasonic waveform is calculated, in which the first peak corresponds to the Time of Flight (ToF). With the identified ToF of 3.987 μs and the nominal velocity of 5.94 mm/μs, the thickness of the specimen is calculated as follows, which is nearly equal to the known thickness of 11.81 mm.

$$\text{Thickness} = \frac{\text{ToF} \times \text{Velocity}}{2} = \frac{3.987\ \mu\text{s} \times 5.94\ \text{mm}/\mu\text{s}}{2} = 11.84\ \text{mm} \tag{3}$$

This experiment validates the robot's successful operation of ultrasonic thickness measurement and its accuracy on flat surfaces. Although this paper does not report measurements on a curved surface, successful ultrasonic measurements on a curved surface have also been validated (see Data Availability Statement for the article). When the curvature is high on a curved surface, a transducer with a smaller surface area should be selected.

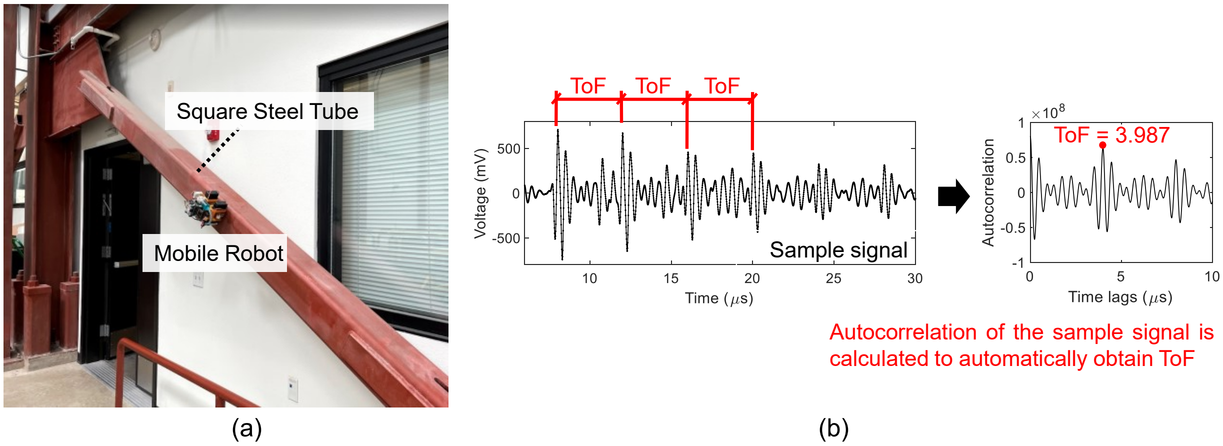

Fig. 14. Ultrasonic thickness measurement on a square steel tube with 11.81-mm nominal thickness; (a) test specimen; and (b) ultrasonic waveform and autocorrelation function

Further validation is conducted on an indoor steel structure as shown in Fig. 15(a). We conduct grid measurements at 12 locations on a channel member, including rusty locations (A4, C1, and C2) and rough spots manually generated by a grinder (B1 and B3). Furthermore, the surface area in the channel for the robot's maneuver is quite limited compared with the previous example. At each of the 12 measurement locations, the ToF is calculated. With the nominal velocity of 5.94 mm/μs, the thickness of each location is obtained, illustrated by the color map in Fig. 15(b). Note that thickness values between two neighboring measurement points are linearly interpolated. Example waveforms at A4 and B1 are also presented in Fig. 15(c). The measured thickness values prove consistent around the nominal value of 16.25 mm, despite slight variations depending on the measurement locations. Moreover, the measured thickness values at B1 and B3, at the manually ground spots, are smaller than other locations, confirming the high-resolution of the measurement by the robotic system.

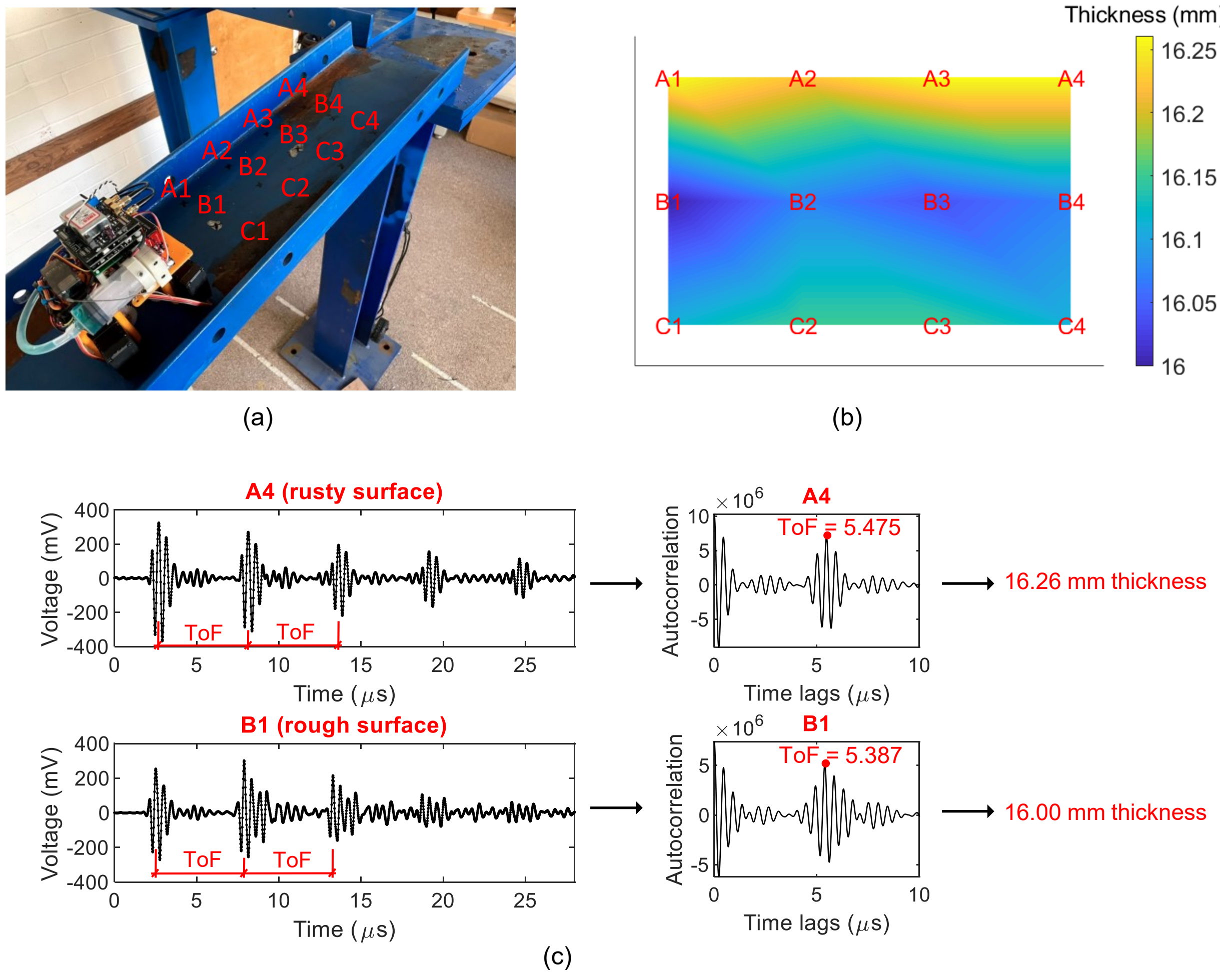

Fig. 15. Grid thickness measurement results: (a) a channel steel member as the test specimen; (b) color map of measured thickness values; and (c) example waveforms and autocorrelation functions at A4 and B1

Real-time visualization of robot position and thickness measurement

Fig. 16 shows an indoor frame structure example that highlights the 3D visualization of the robot path and thickness measurement positions, as well as GoPro camera views. Fig. 16(a)-(c) show a sequence of robot locomotion on the frame structure. Fig. 16(d) shows the 3D visualization of robot path and thickness measurement positions on the ground PC screen. Red dots indicate thickness measurement locations. The thickness values are automatically calculated in real-time by picking up the peak value of the autocorrelation function of ultrasonic waveforms along with Eq. (2). The calculated thickness values are represented by green texts with the unit of inches. The localization enables automatic recording of thickness measurement locations and maps them in 3D space in real-time. Fig. 16(e)-(g) show the GoPro camera view. Depending on whether the robot is traveling or stops for a thickness measurement process, the operator can change the GoPro orientation through the remote controller. This allows the operator to safely navigate the robot to measurement locations (Fig. 16(e)), properly dispense gel couplant (Fig. 16(f)), and firmly press the transducer on a measurement surface (Fig. 16(g)).

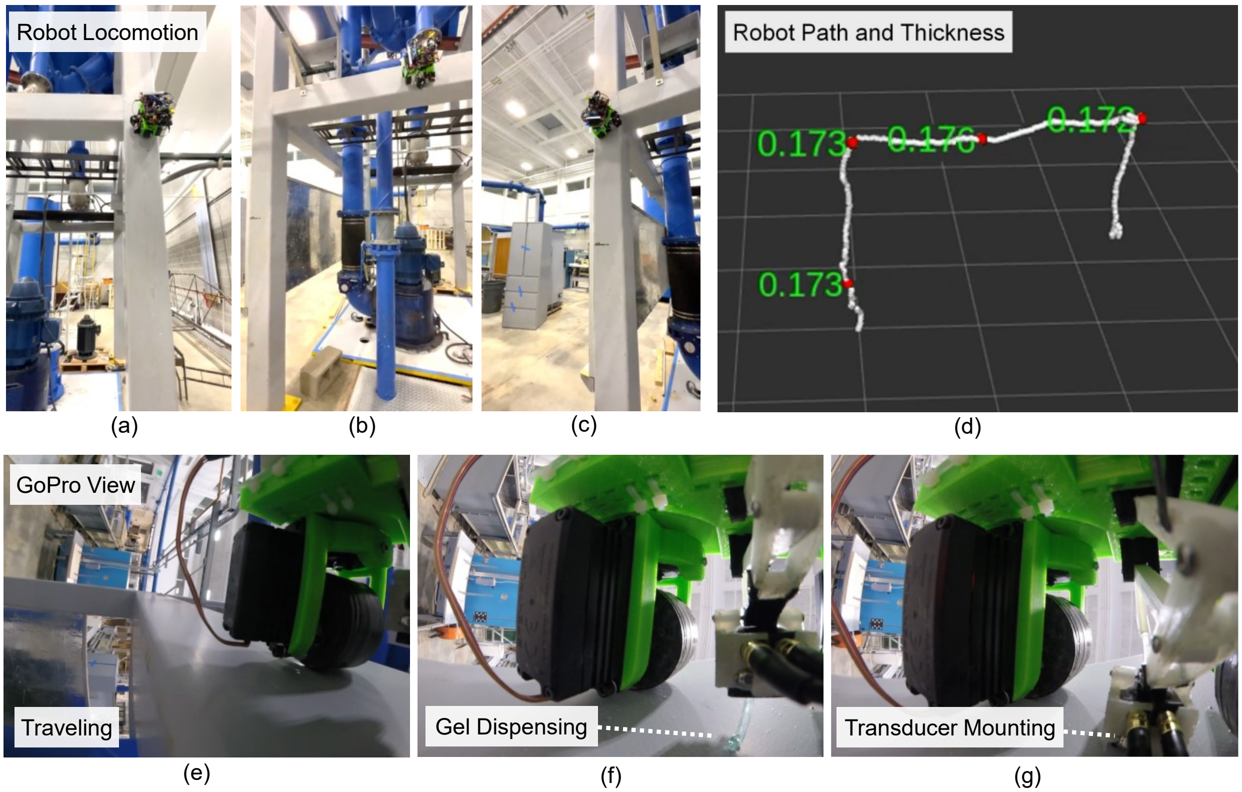

Fig. 16. Indoor frame test: (a)-(c) robot locomotion; (d) real-time visualization of robot path and thickness (unit in inch) in 3D space; and (e)-(g) GoPro camera view

For further validation, we perform a field test on the same steel girder bridge near LaGrange, GA, USA, from Fig. 4. We deploy the robot on the flange and web of the bridge and perform thickness measurements at several locations. Fig. 17 shows the robot locomotion on the flange (Fig. 17(a)) and the web (Fig. 17(b)). Fig. 17(c) visualizes the traveled path and measurement results at three locations (denoted as red dots). The thickness measurements we obtained (0.596 inch, 0.580 inch, and 0.602 inch) on the web are nearly identical with its nominal thickness of 15.24 mm (0.60 inch), which validates the performance of the develop system in a field environment. For more details, please see a video illustration in the Data Availability Statement.

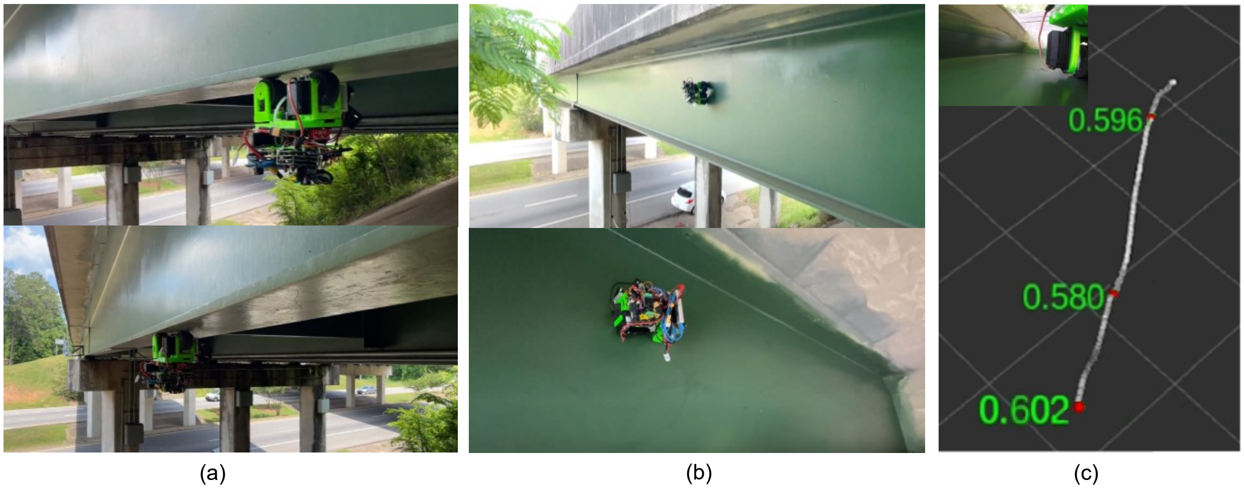

Fig. 17. A field test of the developed mobile robot at a steel bridge girder near LaGrange, GA, USA: (a) locomotion on the flange; (b) locomotion on the web; and (c) thickness measurements on the web (unit in inch)

Conclusion

This paper presents the development of a steel climbing bicycle robot integrated with an ultrasonic sensing device towards autonomous thickness measurement of steel bridge members. The paper first demonstrated the design and field test results of the *Martlet* ultrasonic device, followed by its integration with the bicycle robot along with other sensors. Through several laboratory and field testing, we validated that the developed mobile sensing system can 1) obtain accurate thickness measurements including with rusty and rough surface conditions, 2) assist an operator to safety navigate the robot to measurement locations, properly dispense gel couplant, and firmly press the transducer on a measurement surface, and 3) visualize the robot path and thickness measurement values in 3D space in real-time. A submitted video in the Supplemental Materials provides the illustration of the robot's maneuverability and ultrasonic thickness measurements.

In terms of potential improvements, the current robot can carry gel couplant for about 20 to 30 measurements. As a result, refill is required when more measurements are needed. Elastomer dry couplants can provide an alternative to gel couplant. A study of the use of dry couplant together with an unmanned aerial vehicle has been recently conducted by (Watson *et al.* 2021). Although gel couplant generally produces higher quality ultrasonic signals, it is in our interest to investigate elastomer dry couplant as a possible replacement without sacrificing too much measurement accuracy.

Data Availability Statement

All data, models, or code that support the findings of this study are available from the corresponding author upon reasonable request. Video demonstrating the robot's maneuverability and ultrasonic thickness measurements is available on YouTube: https://youtu.be/aCt0BZnxKVc.

Acknowledgements

This research is partially funded by (i) the U.S. Department of Transportation, Office of the Assistant Secretary for Research and Technology (USDOT/OST-R) under Grant No. 69A3551747126 through INSPIRE University Transportation Center (http://inspire-utc.mst.edu) at Missouri University of Science and Technology; and (ii) the Georgia Department of Transportation (GDOT RP22-02). The first author received scholarship support from the Nakajima Foundation. The authors would like to thank Chuong Le at University of Nevada, Reno for his software supports. Any opinions, findings, and conclusions expressed in this publication are those of the authors and do not necessarily reflect the view of the sponsors.

References

Ahmed, H., La, H. M., and Gucunski, N. 2020. "Review of non-destructive civil infrastructure evaluation for bridges: state-of-the-art robotic platforms, sensors and algorithms." *Sensors*, 20 (14), 3954. https://doi.org/10.3390/s20143954.

Aquil, A., and Leonard, J. B. 2018. *ASM Handbook, Nondestructive Evaluation of Materials*, ASM International, Materials Park, OH, USA.

ASTM-A6/A6M-14. 2014. *Standard specification for general requirements for rolled structural steel bars, plates, shapes, and sheet piling*, ASTM International, West Conshohocken, PA, USA.

Bandyopadhyay, T., Steindl, R., Talbot, F., Kottege, N., Dungavell, R., Wood, B., Barker, J., Hoehn, K., and Elfes, A. 2018. "Magneto: A versatile multi-limbed inspection robot." *Proceedings of the 2018 IEEE/RSJ International Conference on Intelligent Robots and Systems (IROS)*, Madrid, Spain, October 1-5, 2018. https://doi.org/10.1109/IROS.2018.8593891.

Chen, S., Dong, X., Kim, J.-Y., Wu, S., and Wang, Y. 2016. "Design and performance validation of a compact wireless ultrasonic device for localized damage detection." *Advances in Structural Engineering*, 19 (2), 270-282. https://doi.org/10.1177/1369433215624597.

FHWA. 2016. *National Bridge Inventory*, U.S. Department of Transportation, Federal Highway Administration, Washington, DC, USA.

González-deSantos, L. M., Martínez-Sánchez, J., González-Jorge, H., Ribeiro, M., de Sousa, J. B., and Arias, P. 2019. "Payload for contact inspection tasks with UAV systems." *Sensors*, 19 (17), 3752. https://doi.org/10.3390/s19173752.

Horowitz, P., and Hill, W. 1989. *The Art of Electronics*, Cambridge University Press, Cambridge, England.

Kane, M., Zhu, D., Hirose, M., Dong, X., Winter, B., Häckell, M., Lynch, J. P., Wang, Y., and Swartz, A. 2014. "Development of an extensible dual-core wireless sensing node for cyber-physical systems." *Proceedings of SPIE 9061, Sensors and Smart Structures Technologies for Civil, Mechanical, and Aerospace Systems*, San Diego, CA, USA, March 10-13, 2014. https://doi.org/10.1117/12.2045325.

Kulicki, J., Prucz, Z., Sorgenfrei, D., Mertz, D., and Young, W. 1990. *Guidelines for Evaluating Corrosion Effects in Existing Steel Bridges*, Transportation Research Board, Washington, DC, USA.

La, H. M., Lim, R. S., Basily, B. B., Gucunski, N., Yi, J., Maher, A., Romero, F. A., and Parvardeh, H. 2013. "Mechatronic systems design for an autonomous robotic system for high-efficiency bridge deck inspection and evaluation." *IEEE/ASME Transactions on Mechatronics*, 18 (6), 1655-1664. https://10.1109/TMECH.2013.2279751.

Lander, P., Fahed, N., and Wang, Y. 2022. "Martlet wireless sensing system for full scale bridge weigh-in-motion." *Proceedings of SPIE 12046, Sensors and Smart Structures Technologies for Civil, Mechanical, and Aerospace Systems*, Long Beach, CA, USA, March 6-10, 2022. https://doi.org/10.1117/12.2612610.

Liu, X., Dong, X., and Wang, Y. 2016. "Field testing of Martlet wireless sensing system on an in-service pre-stressed concrete highway bridge." *Proceedings of SPIE 2016, Health Monitoring of Structural and Biological Systems*, Las Vegas, NV, USA, March 20-24, 2016. https://doi.org/10.1117/12.2219348.

Malekjafarian, A., Corbally, R., and Gong, W. 2022. "A review of mobile sensing of bridges using moving vehicles: Progress to date, challenges and future trends." *Structures*, 44, 1466-1489. https://doi.org/10.1016/j.istruc.2022.08.075.

Matarazzo, T. J., Kondor, D., Milardo, S., Eshkevari, S. S., Santi, P., Pakzad, S. N., Buehler, M. J., and Ratti, C. 2022. "Crowdsourcing bridge dynamic monitoring with smartphone vehicle trips." *Communications Engineering*, 1 (1), 1-13. https://doi.org/10.1038/s44172-022-00025-4.

Matarazzo, T. J., and Pakzad, S. N. 2016. "Structural identification for mobile sensing with missing observations." *ASCE Journal of Engineering Mechanics*, 142 (5), 04016021. https://doi.org/10.1061/(ASCE)EM.1943-7889.0001046.

Mattar, R. A., and Kalai, R. 2018. "Development of a wall-sticking drone for non-destructive ultrasonic and corrosion testing." *Drones*, 2 (1), 8. https://doi.org/10.3390/drones2010008.

Mazumdar, A., and Asada, H. H. 2009. "Mag-foot: A steel bridge inspection robot." *Proceedings of the 2009 IEEE/RSJ International Conference on Intelligent Robots and Systems (IROS)*, St Louis, MO, USA, October 11-15, 2009. https://doi.org/10.1109/IROS.2009.5354599.

Nguyen, S. T., and La, H. M. 2019a. "Development of a steel bridge climbing robot." *Proceedings of the 2019 IEEE/RSJ International Conference on Intelligent Robots and Systems (IROS)*, Macau, China, November 3-8, 2019a. https://doi.org/10.1109/IROS40897.2019.8967748.

Nguyen, S. T., and La, H. M. 2019b. "Roller chain-like robot for steel bridge inspection." *Proceedings of the 9th International Conference on Structural Health Monitoring of Intelligent Infrastructure (SHMII-9)*, St. Louis, MO, USA, August 4-7, 2019b.

Nguyen, S. T., Nguyen, H., Bui, S. T., Ngo, T. D., and La, H. M. 2022. "An agile bicycle-like robot for complex steel structure inspection." *2022 International Conference on Robotics and Automation (ICRA)*, Philadelphia, PA, USA, May 23-27, 2022. https://doi.org/10.1109/ICRA46639.2022.9812153.

Nguyen, S. T., Pham, A. Q., Motley, C., and La, H. M. 2020. "A practical climbing robot for steel bridge inspection." *Proceedings of the 2020 IEEE International Conference on Robotics and Automation (ICRA)*, Paris, France, May 31- June 4, 2020. https://doi.org/10.1109/ICRA40945.2020.9196892.

Oh, J.-K., Jang, G., Oh, S., Lee, J. H., Yi, B.-J., Moon, Y. S., Lee, J. S., and Choi, Y. 2009. "Bridge inspection robot system with machine vision." *Automation in Construction*, 18 (7), 929-941. https://doi.org/10.1016/j.autcon.2009.04.003.

Otsuki, Y., Lander, P., and Wang, Y. 2021. "Ultrasonic thickness measurement using the Martlet wireless sensing system." *Proceedings of the 2021 International Instrumentation & Measurement Technology Conference (I2MTC)*, Glasgow, Scotland, May 17-20, 2021. https://doi.org/10.1109/I2MTC50364.2021.9460094.

Otsuki, Y., Lander, P., and Wang, Y. 2022a. "Field validation of a compact Martlet wireless ultrasonic thickness measurement system." *Proceedings of the 8th World Conference on Structural Control and Monitoring (8WCSCM)*, Orlando, FL, USA, June 5-8, 2022a.

Otsuki, Y., Nguyen, S. T., La, H. M., and Wang, Y. 2022b. "Autonomous ultrasonic thickness measurement using a steel climbing mobile robot integrated with Martlet wireless sensing." *Proceedings of the 30th ASNT Research Symposium (ASNT30)*, St. Louis, MO, USA, June 20-24, 2022b. https://doi.org/10.32548/RS.2022.029.

Pham, N. H., and La, H. M. 2016. "Design and implementation of an autonomous robot for steel bridge inspection." *Proceedings of the 54th Annual Allerton Conference on Communication, Control, and Computing (Allerton)*, Monticello, IL, USA, September 27-30, 2016. https://doi.org/10.1109/ALLERTON.2016.7852280.

Quigley, M., Conley, K., Gerkey, B., Faust, J., Foote, T., Leibs, J., Wheeler, R., and Ng, A. Y. 2009. "ROS: an open-source Robot Operating System." *ICRA Workshop on Open Source Software*, Kobe, Japan, May 12-17, 2009.

Sirken, A., Knizhnik, G., McWilliams, J., and Bergbreiter, S. 2017. "Bridge risk investigation diagnostic grouped exploratory (BRIDGE) bot." *Proceedings of the 2017 IEEE/RSJ International Conference on Intelligent Robots and Systems (IROS)*, Vancouver, Canada, September 24-28, 2017. https://doi.org/10.1109/IROS.2017.8206562.

Sutter, B., Lelevé, A., Pham, M. T., Gouin, O., Jupille, N., Kuhn, M., Lulé, P., Michaud, P., and Rémy, P. 2018. "A semi-autonomous mobile robot for bridge inspection." *Automation in Construction*, 91, 111-119. https://doi.org/10.1016/j.autcon.2018.02.013.

Wang, Y., Lander, P., Myung, H., and Song, W. 2022. "Robotic sensing for assessing and monitoring civil infrastructures." *Sensor Technologies for Civil Infrastructures*, Woodhead Publishing Cambridge, U.K. https://doi.org/10.1016/B978-0-08-102706-6.00010-6.

Ward, P., Manamperi, P., Brooks, P., Mann, P., Kaluarachchi, W., Matkovic, L., Paul, G., Yang, C., Quin, P., and Pagano, D. 2014. "Climbing robot for steel bridge inspection: design challenges." *Proceedings of the 9th Austroads Bridge Conference*, Sydney, Australia, October 22-24, 2014.

Watson, R., Kamel, M., Zhang, D., Dobie, G., MacLeod, C., Pierce, S. G., and Nieto, J. 2021. "Dry coupled ultrasonic non-destructive evaluation using an over-actuated unmanned aerial vehicle." *IEEE Transactions on Automation Science and Engineering* https://doi.org/10.1109/TASE.2021.3094966.

Zhang, D., Watson, R., Dobie, G., MacLeod, C., and Pierce, G. 2018. "Autonomous ultrasonic inspection using unmanned aerial vehicle." *2018 IEEE International Ultrasonics Symposium (IUS)*, Kobe, Japan, October 22-25, 2018. https://doi.org/10.1109/ULTSYM.2018.8579727.

Zhang, D., Watson, R., MacLeod, C., Dobie, G., Galbraith, W., and Pierce, G. 2022. "Implementation and evaluation of an autonomous airborne ultrasound inspection system." *Nondestructive Testing and Evaluation*, 37 (1), 1-21. https://doi.org/10.1080/10589759.2021.1889546.

Zhou, H., Lynch, J., and Zekkos, D. 2022. "Autonomous wireless sensor deployment with unmanned aerial vehicles for structural health monitoring applications." *Structural Control and Health Monitoring*, 29 (6), e2942. https://doi.org/10.1002/stc.2942.

Zhu, D., Guo, J., Cho, C., Wang, Y., and Lee, K.-M. 2012. "Wireless mobile sensor network for the system identification of a space frame bridge." *IEEE/ASME Transactions on Mechatronics*, 17 (3), 499-507. https://doi.org/10.1109/TMECH.2012.2187915.